UNIVERSITY OF CALIFORNIA,
IRVINE

Single-Molecule Studies of Antibody Binding Using Carbon Nanotube Transistors

THESIS

submitted in partial satisfaction of the requirements
for the degree of

MASTER OF SCIENCE

in Physics

by

Calvin James Lau

Thesis Committee:
Professor Philip G. Collins, Chair
Professor Zuzanna S. Siwy
Assistant Professor Albert Siryaporn

2019

DEDICATION

To

my parents,

for instilling in me a love for learning, a conviction to know the truth, and the skills to succeed;

my friends,

for grounding me in reality and encouraging me during the hard times;

and, most importantly, God,

for giving me life and strength for each day.

TABLE OF CONTENTS

LIST OF FIGURES

ACKNOWLEDGMENTS

I would like to express gratitude and appreciation to my committee chair, Professor Philip G. Collins, who was an indispensable source of guidance and insight for this work. Without the structure, focus, and vision that he provided, along with his hard work and dedication to the lab and his students, none of this would be possible.

I would like to express special appreciation and thanks to Dr. Wonbae Lee, who was an instrumental partner for this research. His hard work, experience, and patience were invaluable in collecting the data and making everything work.

I want to thank the various members and alumni of the Collins research group for their contributions to the lab infrastructure over the years, and to thank, in particular, Dr. Patrick Sims and Dr. Max Akhterov, who took on the responsibility of my training, and Arith Rajapakse, who faithfully fabricated CNT devices for the group for many years. Additional thanks to Mackenzie Turvey, Dr. Davil Garcia, and Dr. Tetyana Ignatova for their insight, training, advice, and encouragement during the period of this work. I would also like to thank Dr. Mark Richardson, Dr. Mariam Iftikhar, and Professor Gregory A. Weiss from the Weiss group, who gave crucial support and insight regarding the chemistry perspective.

Financial support was provided by the University of California, Irvine and Autotelic, Inc.

ABSTRACT OF THE THESIS

Single-Molecule Studies of Antibody Binding Using Carbon Nanotube Transistors

By

Calvin James Lau

Master of Science in Physics

University of California, Irvine, 2019

Professor Philip G. Collins, Chair

Monoclonal antibodies are being increasingly utilized as highly-specific sensing elements and linkers for biosensing and chemical detection applications. Ideally, such sensors would demonstrate a real-time response to analyte concentration, but devices incorporating antibodies are often limited by the kinetics of antibody-antigen binding, which can take tens of minutes to measure accurately. Fast, single-molecule techniques show potential for reducing measurement time and revealing kinetics that are otherwise hidden during ensemble measurements. In this work, field effect transistors (FET) based on carbon nanotubes were used to record the binding activity of antibody 3C6 molecules with paclitaxel at the microsecond timescale. Single-molecule measurements revealed individual antibody-antigen binding and unbinding events, with statistics correlated to paclitaxel concentration, while ensemble measurements exhibited no consistent dependence on paclitaxel concentration. Further analysis of the single-molecule binding statistics showed deviations from simple receptor-ligand binding, suggesting the presence of cooperative binding dynamics between the individual binding sites on the 3C6 molecule. The measurement accuracy of the binding dynamics was limited by bandwidth, suggesting

that measurements performed at higher bandwidth could increase the accuracy of the binding kinetics values obtained. Equilibration times for the single-molecule carbon nanotube FETs were under 60 seconds, demonstrating rapid response times that can be used in real-time sensing applications.

CHAPTER 1

Introduction

Over the last 30 years, monoclonal antibodies have become a ubiquitous tool for producing molecules, devices, and systems that possess specificity, natural or engineered, for a particular substance (1) Though medical researchers first pursued antibody therapy for the treatment of infectious diseases (2), others soon began to use monoclonal antibodies in applications ranging from simple selective linker molecules (3) to biochemical sensors (4).

Paclitaxel, also known by its trademark name Taxol®, is used for the treatment of breast, ovarian, lung, and other types of solid tumor cancers, and as such is included on the World Health Organization's List of Essential Medicines (5). Though an effective chemotherapy drug, paclitaxel's poor solubility in the bloodstream complicates drug delivery and dosage control, leading to variations in effective dosage and producing unnecessarily severe side effects (6). Many of these side effects are due to its delivery vehicle, Cremophor EL, a polyoxyethylated castor oil with its own toxic effects and which also forms micelles in the bloodstream, trapping paclitaxel inside. Experiments using the weakly interacting monoclonal antibodies (3C6 and 8A10) show partial inhibition of paclitaxel's toxicity (7), demonstrating these antibodies' selectivity for the drug and their potential use as molecular sensors for paclitaxel concentration (8). However, commercially-available antibodies, even monoclonal antibodies, suffer from batch-to-batch variation (9) in binding kinetics and affinity, which reduces the precision of antibody-based sensors. Such variation may even

exist from molecule to molecule, suggesting the need for single-molecule studies of antibody binding.

Currently, studies of antibody-antigen binding are often performed as ensemble measurements, whether through surface plasmon resonance (SPR) (10), Raman or FTIR spectroscopy (11), or nuclear magnetic resonance (NMR) spectroscopy (12). These techniques, though useful for characterizing antibody selectivity, do not have the sensitivity to observe the dynamics of an individual antibody molecule. Experiments with single molecule sensitivity utilize atomic force microscopy (AFM) (13) or, more recently, single-molecule Förster resonance energy transfer (smFRET) (14), which is dependent on fluorophores to generate its signal. Fluorophores commonly emit intermittently and with limited photon fluxes, restricting the time resolution that smFRET can achieve, and the fluorophores' tendency to photobleach places an upper limit on the observation time. With such limitations, smFRET cannot determine the presence or absence of sub-millisecond transient events or intermediate states.

Our previous work demonstrated an electronic, label-free technique for monitoring and deciphering enzymatic processing and kinetics with single-molecule resolution, using T4 lysozyme (15) and DNA polymerase I (16) as examples. In those experiments, we tethered the protein to a single-walled carbon nanotube field-effect transistor (SWCNT-FET), then applied a source-drain bias to the CNT and observed the protein's activity via fluctuations in the transistor conductance. These experiments confirmed that this method observes signals

that are correlated to the actual protein behavior (17), and our results matched those of previous studies of the same enzymes using different methods.

In this work, we utilized our electronic observation method to record the binding activity of antibody 3C6 with its target antigen, paclitaxel. Using our SWCNT-FET device, we performed both ensemble and single-molecule measurements, obtaining both time-averaged current versus liquid gate potential (henceforth termed I-V_{lg}) curves and also constant liquid-gate-potential, temporal current recordings (henceforth termed $I(t)$). We demonstrated that the time-averaged I-V_{lg} curves did not show any consistent concentration-dependent shifts but that the temporal recordings showed concentration-dependent rates of binding events. Analysis of the temporal single-molecule recordings showed that the 3C6-paclitaxel complex approximated a two-state system and exhibited concentration-dependent single-molecule binding kinetics that correlated with ensemble binding kinetics obtained in other experiments.

CHAPTER 2

Experimental Methods

SWCNT Synthesis and Device Fabrication

The SWCNT-FET devices were fabricated by depositing metal electrodes by photolithography and electron beam evaporation onto CNTs grown across 4" SiO_2/Si wafers using a chemical vapor deposition (CVD) apparatus. During the CVD process, the CNTs grew as the carbon feedstock, methane, decomposed into amorphous carbon and nucleated around uniformly distributed Fe-Mo catalyst particles. Photoresist was deposited by spin coating onto the wafer, and then the resist layer was patterned through UV exposure. Subsequent metal deposition and resist etching produced SWCNT-FET devices, comprising of a SWCNT covered by two electrodes.

Each device on the wafer was probed to electrically characterize all of the CNT connections between electrodes. Individual SWCNT-FET devices exhibiting an on-resistance of 100-500 kΩ and a current on:off ratio of > 100:1 were selected. Each chip was cleaned with Remover PG heated to 60°C (MicroChem) to remove as much leftover photoresist as possible. A ~300nm layer of Poly(methyl methacrylate) (PMMA) (A3 PMMA, MicroChem) was spin coated onto the chip surface to electrically and mechanically isolate the metal electrodes from any solutions or analytes. The PMMA-covered SWCNT was uncovered by using electron beam lithography to create a 1μm-wide trench in the gap between electrodes, exposing only the SWCNT sidewall. A model of the SWCNT-FET is illustrated in Figure 1A.

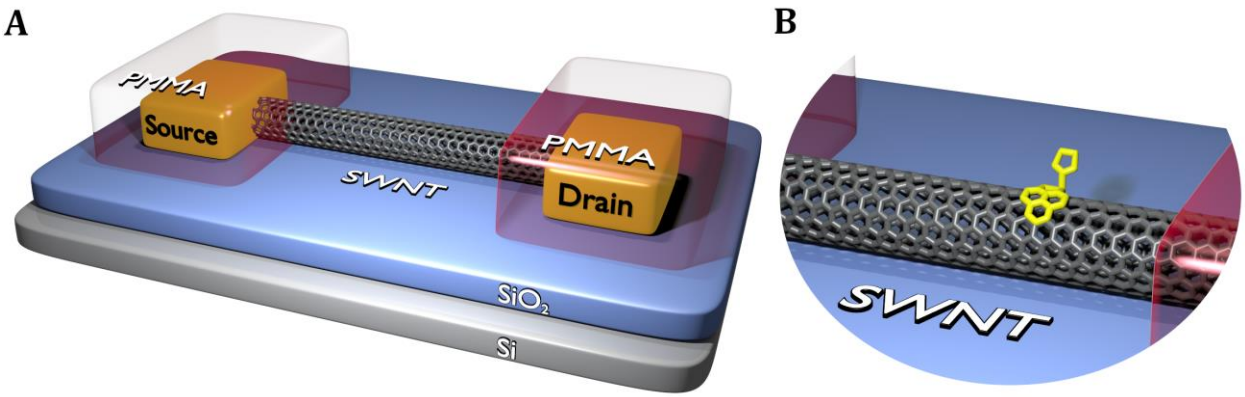

Figure 1: (A) Model of the SWCNT-FET device, with the SWCNT in the center resting on the surface of the Si wafer. Electrodes (colored gold) contact the SWCNT sidewall, and are passivated by PMMA. (B) Close-up view of a pyrene-maleimide linker molecule attached to the SWCNT sidewall.

The resulting SWCNT-FET device was electrically characterized in phosphate-buffered saline (pH 7.3, hereafter called PBS) solution (procedure identical to that outlined below), to test for random telegraph signal (RTS) noise in the device. Any device demonstrating RTS noise before any antibody attachment was discarded.

Ensemble SWCNT devices were created using CNTs from solution. Solubilized CNTs (NanoIntegris) were deposited onto a wafer by spin coating, leaving a dense film of randomly-oriented CNTs on the wafer surface. Deposition of metal electrodes on top of this film produced carbon nanotube network field effect transistors (CNTN-FETs). Subsequent electrical characterization showed that these devices were p-type transistors with lower on/off current ratios (~4-10) than the single-SWCNT-FETs, due to the presence of a few metallic CNTs in the solution mixture. The CNTN-FETs were covered with PMMA, then portions of the PMMA in the gap between electrodes were removed to expose the CNT network.

3C6 Antibody Attachment

N-(1- pyrenyl)maleimide (Sigma-Aldrich) (hereafter called pyrene-maleimide) was used as a linker molecule to anchor the 3C6 antibody to the SWCNT sidewall. The pyrene group of this molecule, consisting of four fused benzene rings, non-covalently bonded to the SWCNT sidewall by π-π stacking, while the maleimide group formed stable thioether bonds with the free thiol of a cysteine on the antibody molecule (18). A solution of 1mM pyrene maleimide in ethanol was prepared. 40 μL of this solution was pipetted onto the top surface of the PMMA-covered chip, which was then left at room temperature (~22°C) for 30 min. The chip was rinsed under a flowing solution of 0.1% Tween-20 (MP Biomedicals) in ethanol for 5s, then rinsed under flowing DI water for another 5s, to remove any excess pyrene maleimide. Figure 1B shows a cartoon of the pyrene maleimide linker molecule attached to the CNT sidewall.

3C6 antibodies were attached to the SWCNTs in solution. Anti-SA2 antibody [3C6] (ab117725) (Autotelic + Abcam), a monoclonal human IgG1 antibody, was diluted to 53 nM in PBS buffer, then divided into 60 μL aliquots and frozen for storage. When needed, the 3C6 aliquot was thawed and pipetted onto the top surface of the chip, and the chip was left at room temperature (~22°C) for 30 min. This concentration was chosen to facilitate, on average, one attachment per SWCNT. The chip was rinsed under a flowing solution of 0.1% Tween-20 in PBS solution for 5s, then rinsed under flowing DI water for another 5s, to remove any excess 3C6 from the chip surface. The chip was submerged in PBS solution at room temperature (~22°C) for short-term storage.

Electrical measurements

All electrical measurements were performed with the 3C6 molecule and exposed SWCNT sidewall (the active portion of the device) submerged in solution. The solution potential was maintained by platinum reference and counter electrodes, with the voltage between the reference electrode and the SWCNT (hereafter called liquid-gate voltage, or V_{lg}) maintained by a Keithley 2400 SourceMeter. The back gate (back surface of the device) was maintained at ground (0 V), and a voltage (V_{sd}) was applied between the source and drain electrodes on the chip surface. The source-drain current ($I(t)$) was amplified by a Keithley 428 current amplifier set to a gain of 10^8 V/A (with a 10%-90% rise time of 40 μs), and the resulting signal was acquired by a National Instruments DAQ card (PCI-6281).

Measurements were taken first in PBS solution as a control. Generally, carbon nanotube transistors have inherent 1/f (pink) noise (19), and sometimes also exhibit random telegraph switching (RTS) noise (20, 21) without any additional molecules attached. The RTS noise is generally caused by defects in the SWCNT, charge traps in the underlying SiO_2 substrate on which the CNTs are fabricated, or impurities at the CNT-metal contact. Unfortunately, RTS noise can appear similar to the signal generated by 3C6 binding and unbinding. Thus, any SWCNT-FET/3C6 complex that exhibited such RTS before exposure to paclitaxel was excluded from further measurement and analysis.

The target antigen, paclitaxel (Autotelic), was dissolved in solution before being applied to the devices. Solutions were prepared by pipetting small amounts of the storage solution (6

mg/mL of paclitaxel dissolved in polyoxyethylated castor oil and dehydrated alcohol) into PBS buffer to produce the target concentrations. The paclitaxel solutions were prepared fresh within 2-3 hours of each measurement, since the low solubility of paclitaxel in aqueous solutions caused it to precipitate out of solution over time (22).

Measurements were then performed in approximately logarithmically-spaced concentrations of paclitaxel in PBS solution ranging from 20 pM to 200 nM. For each concentration, a $I\text{-}V_{lg}$ curve ($0.6V < V_{lg} < 0.4V$) was first acquired, obtaining time-averaged measurements with each point being an average of 0.5s of data at 5 kHz. Such $I\text{-}V_{lg}$ measurements correspond to those performed by other CNT biosensor experiments (23). Then, the V_{lg} was held constant, and $I(t)$ was measured for a minimum of 300s at an acquisition rate of 100 kHz. After completing recordings for a particular solution, the chip was rinsed under flowing DI water for 5s, then submerged in PBS solution until the next measurement. After all electrical measurements were completed, the device was rinsed under running DI water for 5s and then dried with a compressed air gun.

Imaging

Atomic force microscopy (AFM) (Pacific Nanotechnology Nano-R) was used to determine how many 3C6 antibodies were attached to the SWCNT. Attached 3C6 appeared as ~3nm-high dots overlapping with the line of the SWCNT, which is consistent with the approximate size of the 3C6 molecule (13).

The AFM images were used to categorize devices according to the number of SWCNTs and the number of attached 3C6 molecules. The categories were: single-SWCNT and single-3C6 (single-molecule device, Figure 2A), single-SWCNT and multiple 3C6 (few-molecule device, Figure 2B), and multiple-SWCNT and multiple 3C6 (ensemble device, Figure 2C).

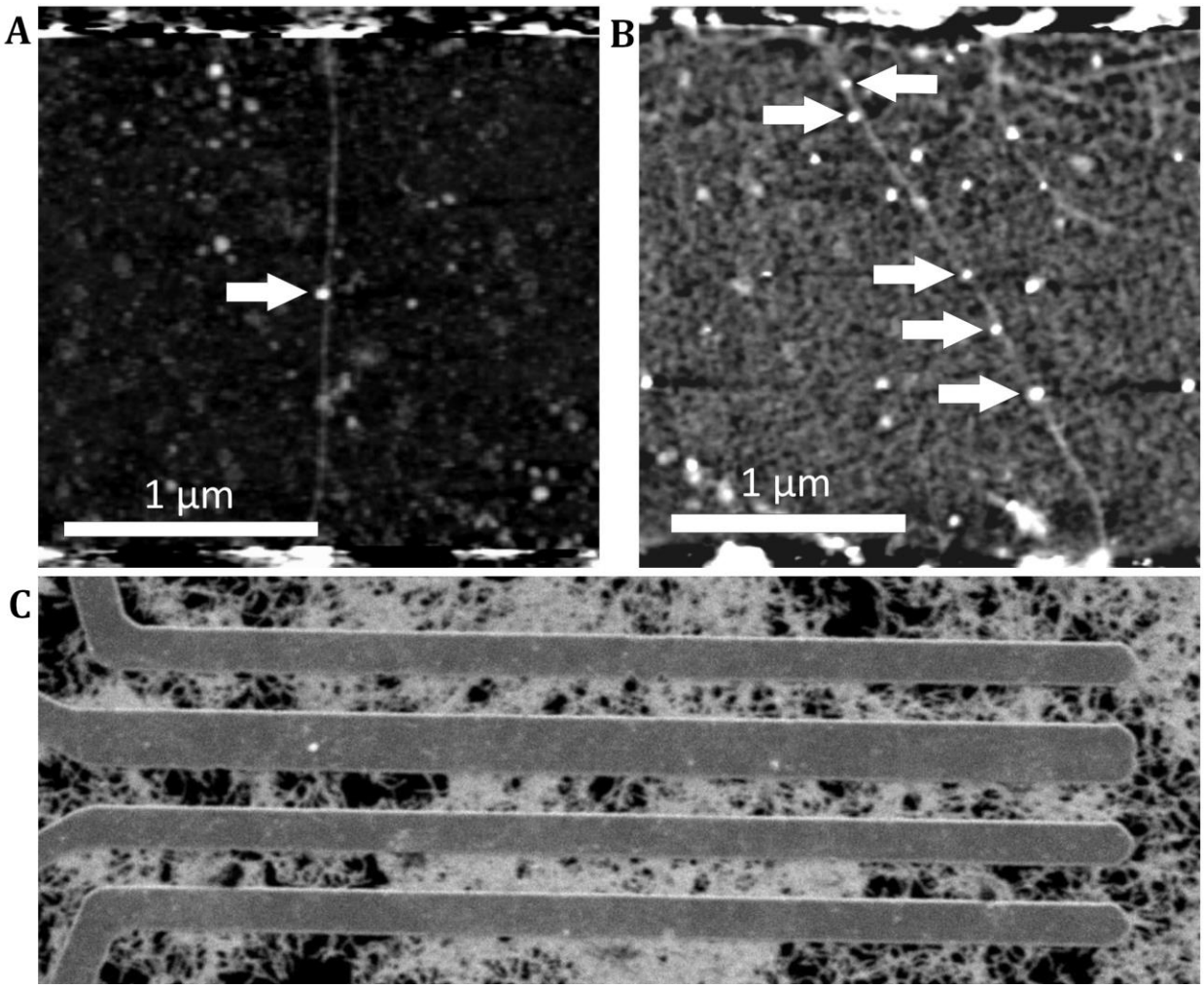

Figure 2: (A) Atomic force microscopy (AFM) image of a single-molecule device. The individual 3C6 molecule appears as a dot (shown with an arrow) overlapping with the line of the SWCNT, here shown running down the middle of the image. (B) AFM image of a few-molecule device, with arrows pointing to multiple attached 3C6 molecules. (C) Scanning electron microscopy (SEM) image of several ensemble devices, where each device is composed of two adjacent electrodes (gray) connected by a network of CNTs (white). The individual 3C6 molecules are not visible with this imaging technique.

Signal Analysis

The obtained I-V_{lg} curves were normalized to allow comparison of curves resulting from different paclitaxel concentrations and to quantify the resulting shifts. First, the I-V_{lg} curves were converted to G-V_{lg} curves by dividing I by V_{sd}. Then, a constant was subtracted from the G-V_{lg} curves to align all of the curves at the right-most end (at V_{lg} = +0.4 V). This was especially important for comparing the G-V_{lg} curves of the ensemble devices, since the CNT networks contained some metallic paths that continued to conduct when all of the semiconducting SWCNTs were turned off (24). G-V_{lg} curves from the same device were plotted together, and shifts in maximum current (measured at V_{lg} = -0.6 V) and entire shifts of the curve itself were calculated.

The raw $I(t)$ signal was converted to a simple binary signal to facilitate two-state analysis. The $I(t)$ signal was converted to conductance using the relation $G(t) = I(t)/V_{sd}$. The entire data set, more than 300s long, was broken up into short segments of ~1-3s. Segments were detrended by subtracting the low frequency noise ($\Delta G(t) = G(t) - \langle G(t) \rangle$, with the average calculated over 100 μs), and then filtered using an implementation of the NoRSE algorithm (25). Each data point in the filtered signal was assigned to either the high or low state using a simple threshold algorithm, with the threshold placed approximately halfway between the two levels of the RTS signal. The threshold algorithm also ignored any events that were shorter than 50 μs to reject spurious event-like noise peaks that were too short to have been amplified by the preamplifier. An example of the binary signal superimposed on the detrended $\Delta G(t)$, showing the accuracy of fitting, is displayed in Figure 3.

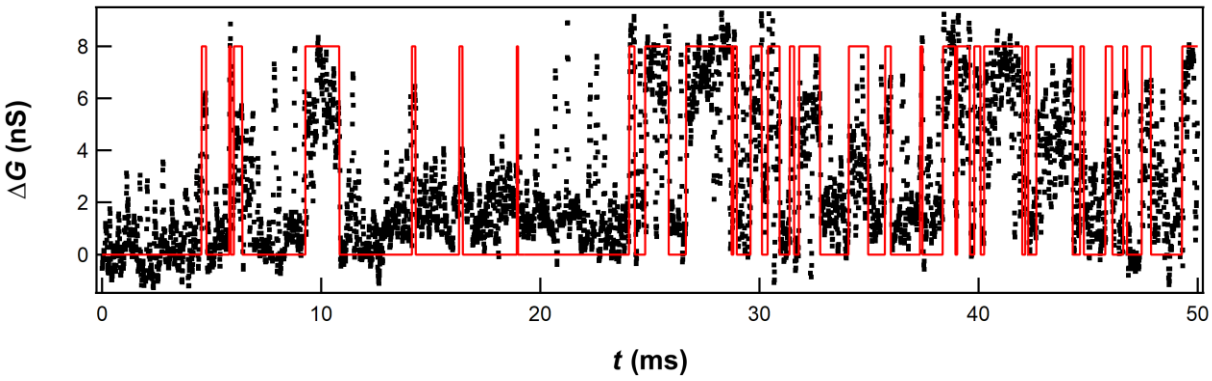

Figure 3: Plot of 50ms of the detrended conductance *G(t)* (black) for a typical single-molecule measurement (in this case at 70nM paclitaxel), with the calculated binary signal shown in red. The conductance jumps between two states (indicated by the two levels of the binary signal). Time durations of individual states are represented by the length of each horizontal line segment.

The duration for each occurrence of the high and low states was calculated. For each concentration and each state, the distribution of the state durations was plotted on a semi-logarithmic histogram, then fitted to a bi-exponential function with zero Y offset. Figure 4 shows an example of the probability distribution, and the corresponding bi-exponential fit, for both the high state and low state. The fitted function appeared approximately piecewise-linear in a semi-log plot, corresponding to a bi-exponential distribution with two characteristic times τ_1 and τ_2. In addition, the arithmetic average time $\langle t \rangle$ of each state was calculated. The average probability of time that the $\Delta G(t)$ signal spent in the high state versus the low state was calculated by normalizing the binary signal to have zero offset and unity amplitude, then taking the average of the normalized signal to obtain the high state average. The number of switches (defined as the number of changes from the low state to the high state) was calculated from the binary signal, and the average switching rate calculated for each concentration.

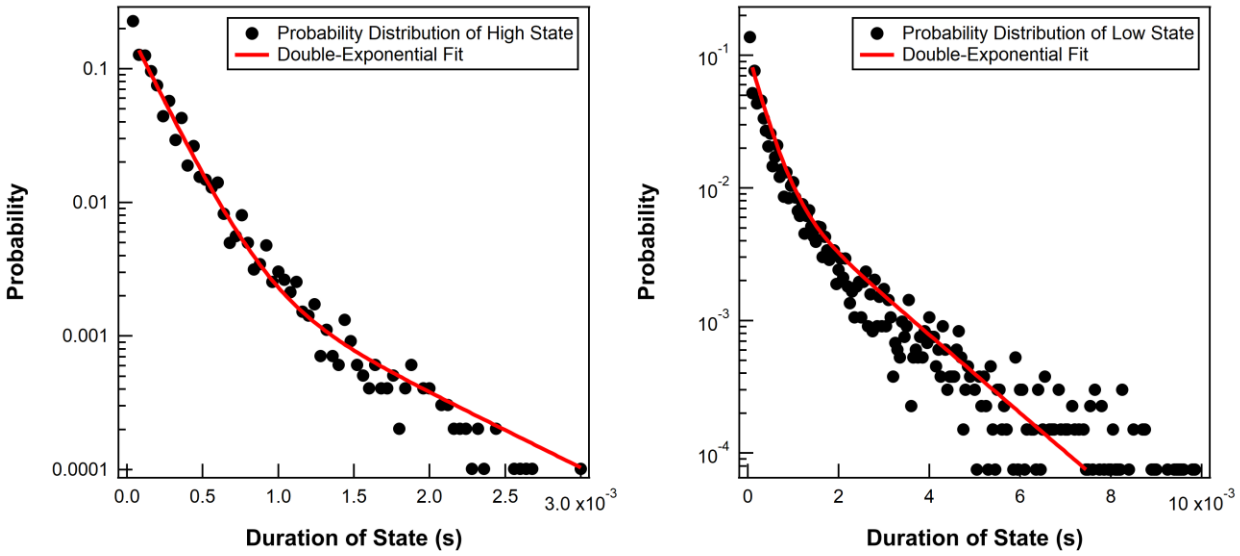

Figure 4: Typical log-linear plots of the probability distributions (black) for both the high state (left) and the low state (right), with the double-exponential fit for each state shown in red. Double-exponential functions appear as approximately piecewise-linear functions with two linear regions corresponding to the two characteristic values, in this case the time constants τ_1 and τ_2.

CHAPTER 3

Electronic Single-Molecule Measurements of the 3C6-Paclitaxel Binding Interaction

Results

Every device showed an immediate and irreversible shift in the G-V_{lg} curve upon the first exposure to paclitaxel. The single-molecule devices gradually equilibrated over 60 seconds, and ensemble devices gradually equilibrated over 120 seconds. The shifts were most visible and uniform for the single-molecule device, for which the electrostatics of the attached 3C6 were most predictable. For these devices, the curve uniformly dropped to ~80% of the pre-exposure value over the entire V_{lg} range (Figure 5A). The curves for the few-molecule devices became less steep but shifted right by ~250 mV, causing the current to decrease for most V_{lg} < -0.4 V and increase for -0.4 V < V_{lg} < -0.1 V (Figure 5B). The response of ensemble devices was least predictable (Figure 5C). Attempts to rinse away the paclitaxel, however, had negligible effect on the G-V_{lg} curves, and subsequent exposures never produced a response as large as the initial exposure. Furthermore, these subsequent shifts were not concentration dependent. Figure 5C shows an example of a non-monotonic response, where I was reduced by the presence of paclitaxel, but by different amounts that did not necessarily correlate with concentration.

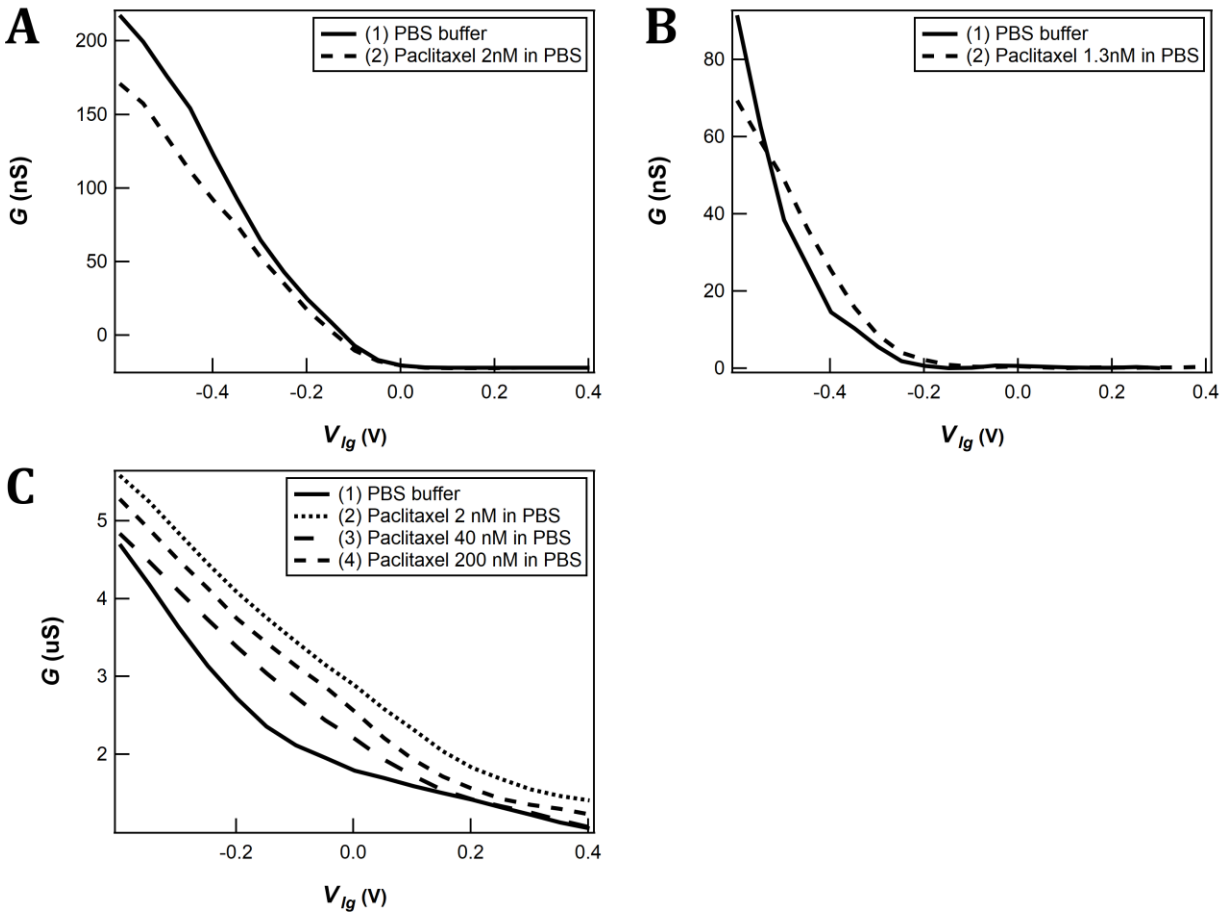

Figure 5: Plots of a typical G-V_{lg} curve for a (A) single-molecule device, (B) few molecule device, and (C) ensemble device, with measurement in buffer shown by a solid black line and measurements with paclitaxel shown as various dashed or dotted black lines. The number in parenthesis in each plot legend indicates the order of the measurement.

The shift in the G-V_{lg} curve was also accompanied by single-molecule fluctuations $\Delta G(t)$ associated with paclitaxel binding and unbinding. Figure 6 shows typical graphs of $\Delta G(t)$ for the three types of devices. The single-molecule devices gave the simplest signals consisting of stochastic fluctuations between only two states. This two-level switching was consistent with the presence of a single 3C6 binding site and also with previous experiments labeling SWCNTs with single biomolecules (15, 16). The few-molecule devices displayed various combinations of two-level, three-level, or multi-level fluctuations that were consistent with

one or more active 3C6 antibodies. Assuming each 3C6 molecule behaved independently, multiple 3C6 molecules were expected to contribute additively to the *G(t)* signal, so these multi-level signals displayed the activity of multiple 3C6 molecules. In the extreme case of ensemble devices, Δ*G(t)* signals no longer displayed clearly-resolvable states, most likely because of the averaging and incoherence of multiple active sites. With all the devices, Δ*G(t)* fluctuations disappeared when the paclitaxel was rinsed away, even though the shifts in *G-V*$_{lg}$ curves were not entirely recovered. The difference suggested that part of the shift was caused by nonspecific binding to the surface or the CNT sidewall, whereas the Δ*G(t)* fluctuations were driven by specific binding to the 3C6 antibodies.

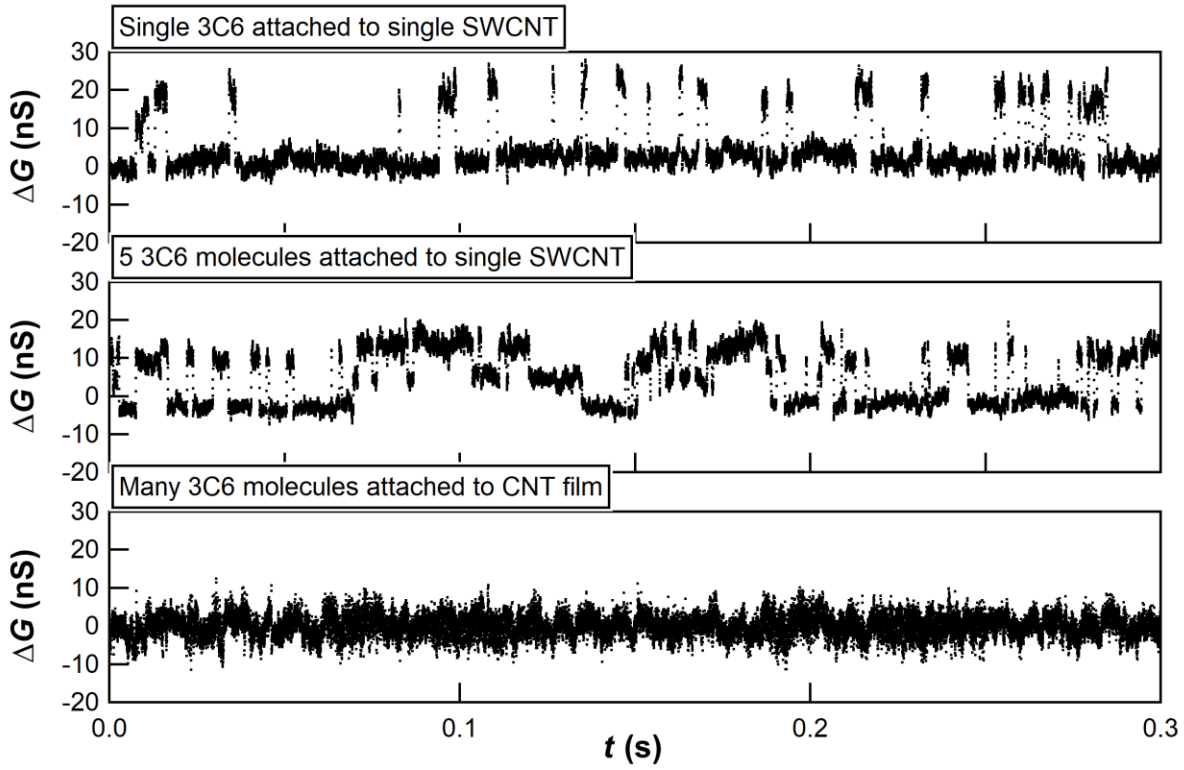

Figure 6: Plots of typical Δ*G(t)* recordings for single-molecule (top), few-molecule (middle), and ensemble (bottom) devices. Single-molecule devices showed clear two-level switching, few molecule devices sometimes showed multi-level switching, and ensemble devices showed no clear switching.

Each discrete level in $\Delta G(t)$ was interpreted as being caused by one active 3C6. However, the number of levels did not exactly match the number of 3C6 attachments observed by AFM. Sometimes, devices with 2-4 attached 3C6 molecules produced a simple, RTS signal consistent with only 1 active binding site. Other such devices produced complex $\Delta G(t)$ signals with multiple levels or complex noise. This demonstrated that not all 3C6 molecules were active and able to produce an electrical response to paclitaxel binding. Unlike in previous research with single-cysteine mutants, the 3C6 molecule had many cysteine residues exposed, and thus had many possible attachment sites to the SWCNT (26, 27). Figure 7 shows the ribbon diagram of an IgG1 molecule (28), with the individual cysteine residues highlighted in blue. Some of these attachment orientations may have prevented the 3C6 molecule from electrically gating the SWCNT. Further analysis of $\Delta G(t)$ was performed only with the single-molecule devices, which produced the most straightforward signals.

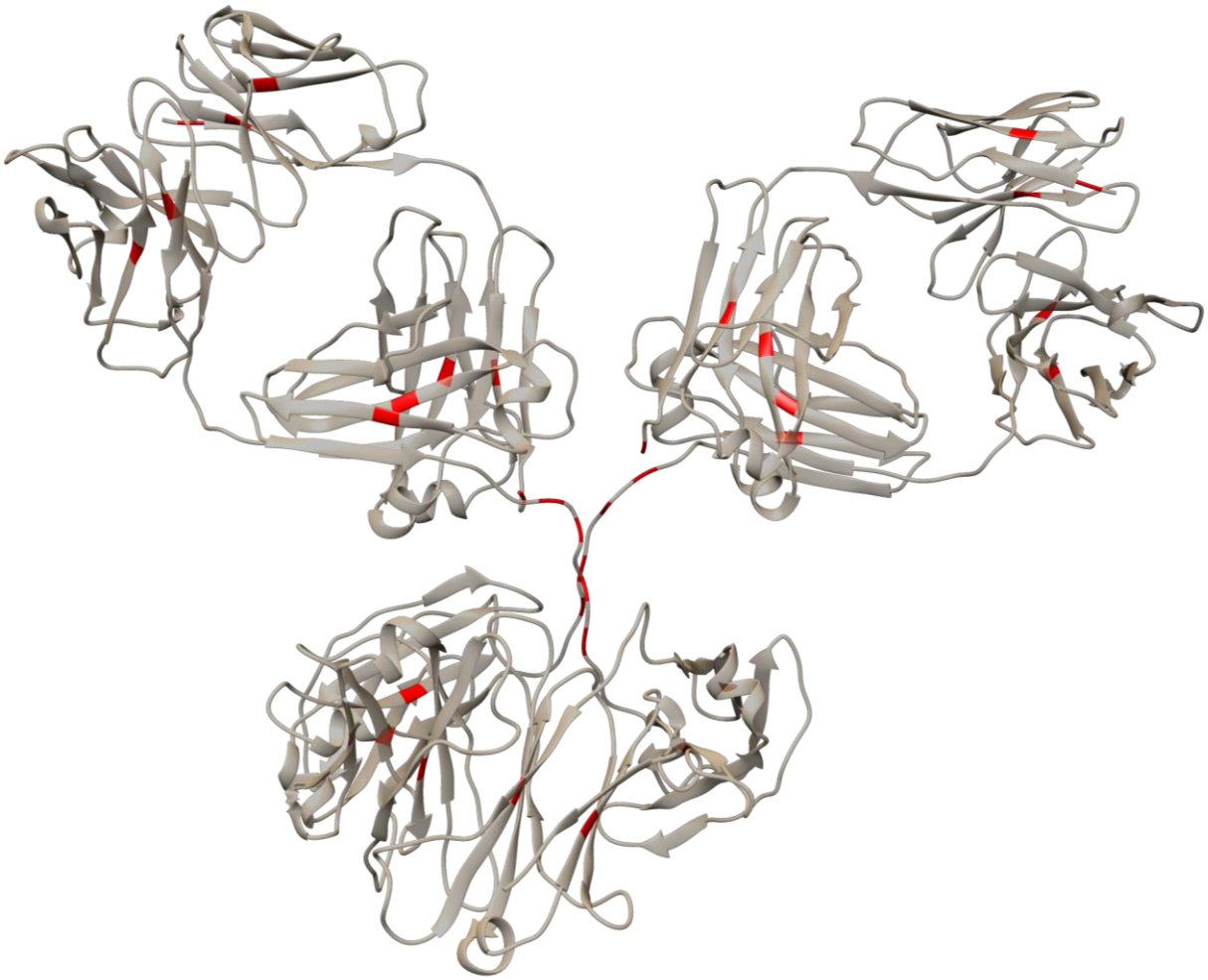

Figure 7: Ribbon structure of an IgG1 molecule, like 3C6, oriented like a letter "Y", with the two binding sites at the top left and right. The cysteine residues are highlighted in red, showing the possible locations for the maleimide-thiol linkage to the SWCNT.

The simple two-level $\Delta G(t)$ signals from the single-molecule devices were analyzed in terms of bound and unbound states. Figure 8 depicts these two states as the two horizontal levels of the red lines to guide the eye. Qualitatively, at lower paclitaxel concentrations, the conductance was mostly in the lower state, with occasional, short jumps into the higher state. At higher concentrations, the behavior was exactly opposite, residing mostly in the higher state and occasionally jumping into the lower state. At concentrations between 10 and 70 nM, the conductance exhibited stochastic, high frequency switching between states and

spent substantial time in both states. The lower state was interpreted as the unbound state, using measurements in low concentration, in which the 3C6 molecule spent most of its time waiting for a paclitaxel molecule to arrive. The high state was interpreted to be the bound state, using measurements in high concentration when the 3C6 molecule was surrounded by large numbers of paclitaxel molecules.

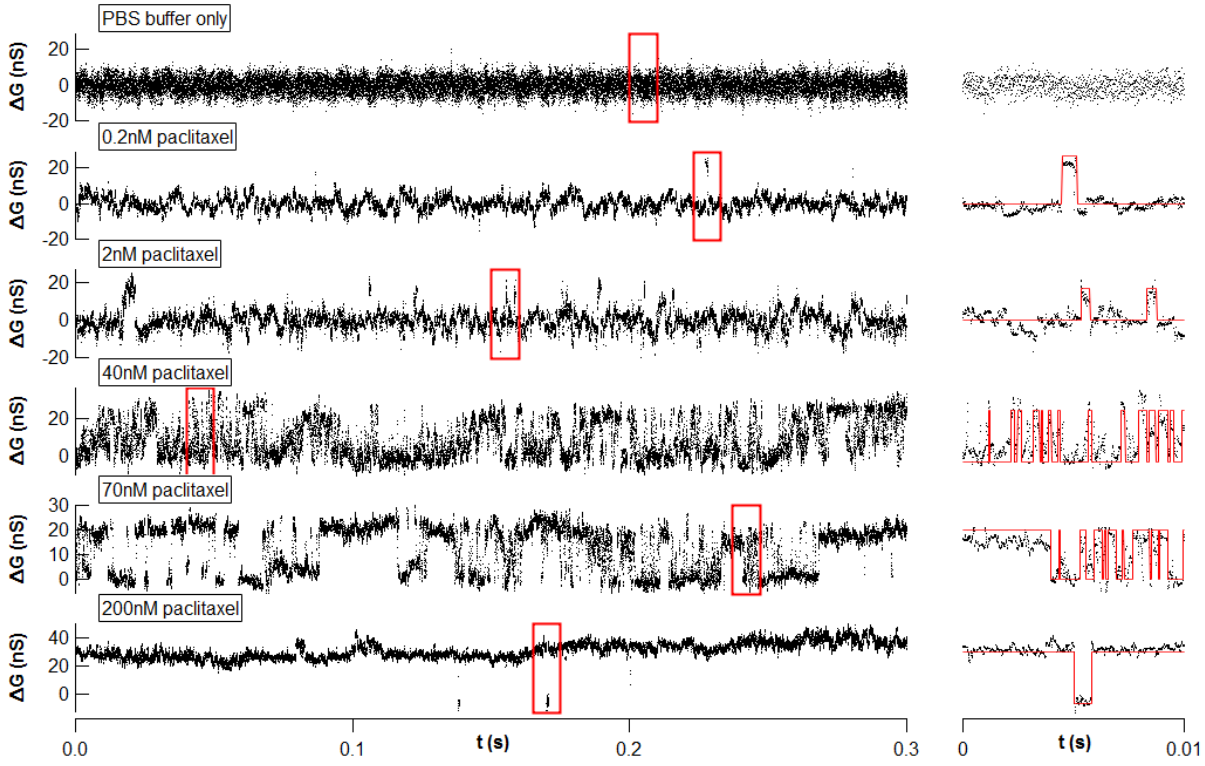

Figure 8: Plots of typical $\Delta G(t)$ recordings for a single-molecule device at various paclitaxel concentrations. The plots on the left are 0.3s of data, and the plots on the right are expanded views of the corresponding regions highlighted by the red boxes (each 0.01s long). The calculated binary signal for each expanded view is shown in red.

Transitions between events were stochastic, approximating a Poisson point process with a time-dependent rate constant $\tau_P(t)$. At any given moment, the distributions of time durations for both the bound and unbound states were approximately Poisson (approximately fit by an exponential function with a characteristic time τ), but the instantaneous binding rate

varied stochastically. Nevertheless, long data records could be accumulated, and the resulting accumulated distribution of the time durations for both the bound and unbound states formed either single or bi-exponentials. Each distribution was described according to two parameters. One was the Poisson time constant τ, which could be considered the most probable binding rate. Since many of the distributions formed bi-exponentials, there were often two τ values for each state, suggesting two independent processes. The other was the arithmetic mean of time durations $<t>$, which incorporated all of the actual deviations from Poisson behavior and could be correlated with the average binding rate as observed by ensemble measurements.

Figures 9A and 9B shows the dependence of the four τ values on paclitaxel concentration. Quantitatively, both $\tau_{unbound1}$ and $\tau_{unbound2}$ decreased consistently over the entire concentration range in a manner approximating a power law. $\tau_{unbound1}$ dropped from $\sim 10^{-1}$ to $\sim 10^{-4}$ s, with an exponent of $\sim$-0.56. $\tau_{unbound2}$ dropped from $\sim 10^{-2}$ to $\sim 10^{-5}$ s, with an exponent of $\sim$-0.71. The fractional exponents obtained here differed from the exponent of unity expected for a second-order reaction in basic receptor–ligand kinetics. This suggested the presence of intermediate steps in the paclitaxel-3C6 binding process, not yet observed, that alter the reaction kinetics to produce the observed fractional reaction order.

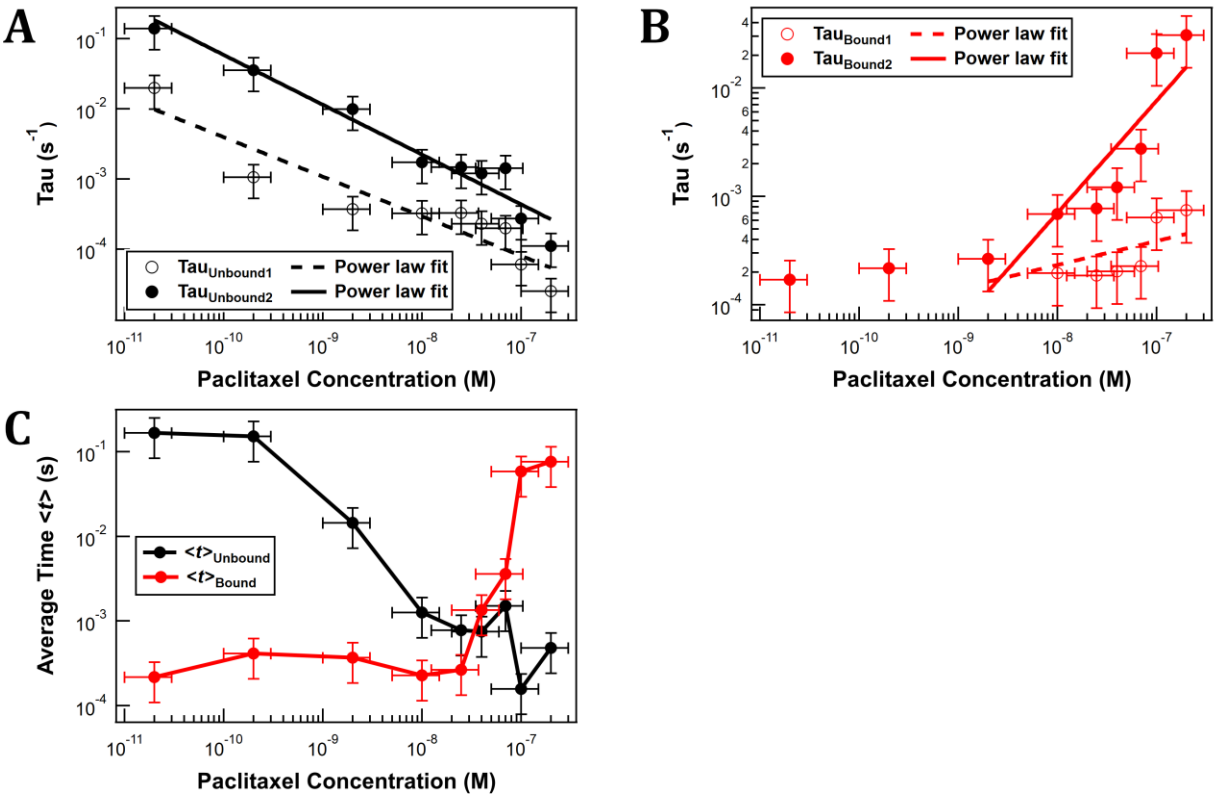

Figure 9: (A) Plot of the dependence of the two $\tau_{unbound1}$ values on paclitaxel concentration. The first value is chosen to always be the larger of the two values. The power-law fits for each value is shown, with the fit for $\tau_{unbound1}$ having a slope of ~-0.56 and the fit for $\tau_{unbound2}$ having a slope of ~-0.71. (B) Plot of the dependence of the two τ_{bound1} values on paclitaxel concentration. The power-law fits for each value is shown, with the fit for τ_{bound1} having a slope of ~+1 and the fit for $\tau_{unbound2}$ having a slope of ~0.22. Below 2nM, the two τ_{bound1} values are identical and approximately constant. (C) Plot of the dependence of <*t*> on paclitaxel concentration.

By contrast, τ_{bound1} and τ_{bound2} demonstrated two distinct regions of concentration dependence. At paclitaxel concentrations below 2 nM, both τ_{bound1} and τ_{bound2} remained approximately constant at ~10^{-4} s. At these concentrations, the resulting distribution of τ_{bound} showed no evidence for a bi-exponential, so the single exponential τ_{bound} was used for both. As paclitaxel concentration increased, the τ_{bound} values separated, with τ_{bound1} remaining relatively constant and τ_{bound2} rising to ~10^{-2} s. In this separated region, τ_{bound1} demonstrated a power law concentration dependence with exponent ~1.0, while τ_{bound2}

demonstrated an exponent of ~0.22. From the definition of the ensemble dissociation constant, $K_d = \frac{1}{K_a} = \frac{k_{off}}{k_{on}}$, and assuming that $k_{off} = \frac{1}{\tau_{bound1}} = 10^4\ \mathrm{s}^{-1}$, the on-rate constant k_{on} was estimated to be: $k_{on} = \frac{k_{off}}{K_d} = \frac{10^4\ \mathrm{s}^{-1}}{10\times10^{-9}\ \mathrm{M}} = 10^{12}\ \mathrm{s}^{-1}\ \mathrm{M}^{-1}$.

Figure 9C shows that $\langle t \rangle_{bound}$ and $\langle t \rangle_{unbound}$ exhibited opposing concentration dependence, each mirroring the other around some crossover concentration value. At paclitaxel concentrations below 10nM, $\langle t \rangle_{bound}$ stayed on the order of 10^{-4} s while $\langle t \rangle_{unbound}$ was roughly 10^{-1} s. At high concentrations, the $\langle t \rangle_{bound}$ and $\langle t \rangle_{unbound}$ values switched in orders of magnitude, such that $\langle t \rangle_{bound}$ rose to around 10^{-1} s and $\langle t \rangle_{unbound}$ dropped to the order of 10^{-3} s. The greater value of $\langle t \rangle$ as compared to τ reflected the more frequent occurrence of longer events than predicted by a purely Poisson point process. These deviations suggested that the bound and unbound states were actually collections of substates arising from dynamic disorder in the 3C6 molecule conformation, perhaps driven by thermal fluctuations. At paclitaxel concentrations around 30nM, both $\langle t \rangle_{bound}$ and $\langle t \rangle_{unbound}$ converged at about 10^{-3} s, indicating some sort of balance between binding and unbinding. This crossover concentration value was in good agreement with the value of K_d=10 nM (8) as found through ensemble measurements of the 3C6-paclitaxel binding interaction.

Figure 10 shows that the time-averaged binding probability was concentration dependent and indicated a similar crossover concentration value. At low concentrations (< 200 pM), the signal resided in the low state for over 99% of the time, whereas at high concentrations (> 100 nM), the signal resided in the high state for over 99% of the time. Between these two

extremes, the probability of the high state increased with concentration in a manner approximating a logarithmic sigmoidal binding curve, with a 50% high state / 50% low state crossing at ~30 nM, fairly close to the ensemble-measured K_d =10 nM. The correlation between the time-averaged binding probability calculated here and the ensemble-measured K_d value for the antibody 3C6-paclitaxel interaction suggested that the ensemble average reflected a simple time-average of the single-molecule binding dynamics for this particular interaction, and that the binding process itself was ergodic. The resulting fit of the data to the Hill equation resulted in a Hill coefficient of ~1.8.

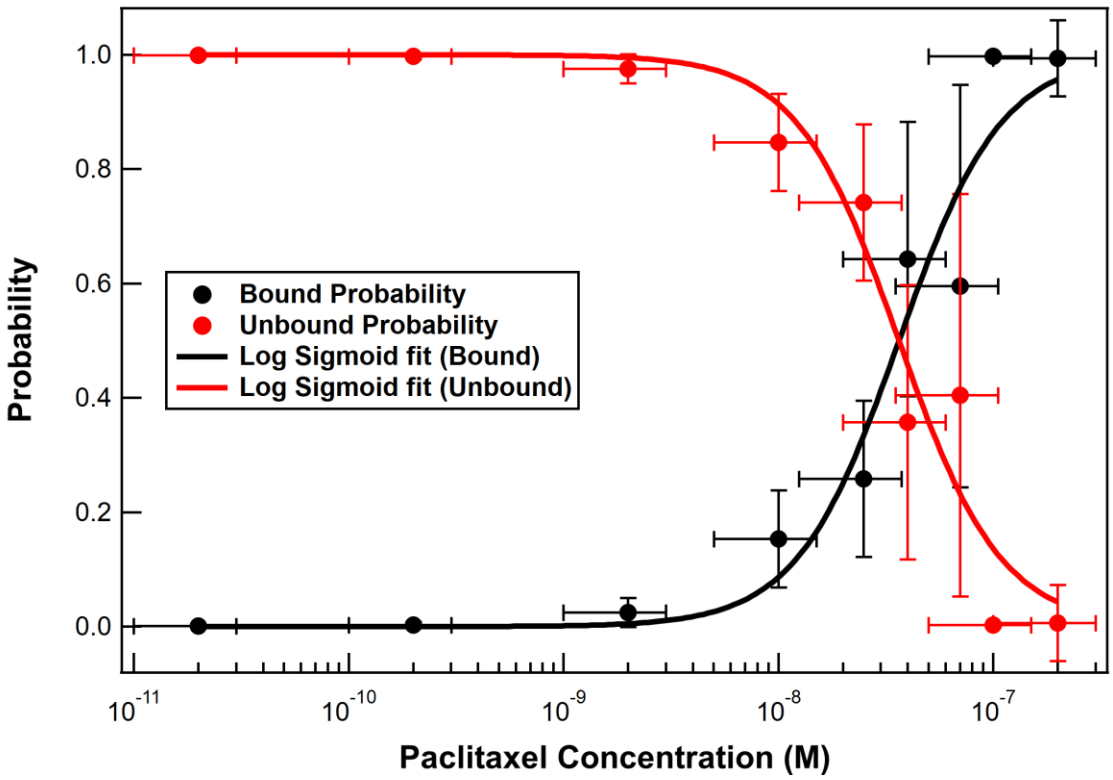

Figure 10: Plot of the overall probability of the bound (high) state (black) and the unbound (low) state (red) as a function of paclitaxel concentration. The corresponding fits to a logarithmic sigmoidal binding curve are shown as solid lines. The 50% bound / 50% unbound crossover point occurs at ~30nM. The Hill coefficient determined by the fit is ~1.8.

Deviations from the exponential fit occurred only at longer time durations, which occurred much less frequently than the short events, and such deviations described events that were longer than what was predicted by the fit. The presence of some very long event times ($\tau >$ 1s) supported the hypothesis that the 3C6 became inactive for certain periods of time.

Discussion

The acquired G-V_{lg} curves were shown to be uncorrelated to the concentration of paclitaxel in solution, even though similar SWCNT-FET devices have been shown to respond predictably to analyte concentration in other studies (23). One possible reason for this discrepancy was nonspecific and irreversible adsorption of paclitaxel on surfaces surrounding the 3C6-SWCNT device. Both paclitaxel and its storage solution, castor oil, are generally insoluble in water (29) and were difficult to reliably rinse away, thus preventing the SWCNT-FET device from returning to the electrostatic condition of a pristine device.

The bi-exponential fit of the unbound time distributions suggested that the mechanism of paclitaxel binding to the 3C6 molecule involved two independent Poisson-like processes. The similar concentration dependence of both $\tau_{unbound1}$ and $\tau_{unbound2}$ suggested that both processes corresponded to actual 3C6-paclitaxel binding events. Perhaps the second process corresponded to paclitaxel attaching to the second antigen binding site on the 3C6 molecule. Despite the two binding sites, the 3C6 molecule did not produce three current levels, which is unlike previously-studied enzymes with multiple ligand binding sites, such as protein kinase A (30). This may have been because the SWCNT-FET biosensor is sensitive to

conformational changes within ~1nm of the CNT sidewall (17). Since the attachment location for the specific 3C6 molecule studied here was unknown, it is possible that the SWCNT biosensor in this case was linked to one of the arms of the 3C6 molecule. Due to the inherent flexibility of antibodies, this would have left the SWCNT biosensor sensitive to the dynamics of one binding site but not the other.

Antibody-antigen interactions are expected to follow general receptor-ligand kinetics, which treat binding as a second-order reaction and unbinding as a first-order reaction. The approximately power-law concentration dependence of both $\tau_{unbound}$ values show similarities to a second-order reaction, but there were significant deviations of the exponents from unity. The approximately constant value of τ_{bound} for concentrations below K_d corresponded to a concentration-independent unbinding rate, which was expected for a first-order reaction. The reason for the abrupt deviations from this constant rate for concentrations above K_d are not conclusively known, but these deviations could be explained by inaccuracies in the measurement or event discrimination algorithm at high event rates, perhaps due to limited measurement bandwidth.

The calculated binding and unbinding rate constants for the 3C6-paclitaxel interaction were eight orders of magnitude faster than the rate constants observed for other antibodies in experiments using ligand binding assays. The 3C6-paclitaxel system was specifically chosen for this experiment because its binding kinetics were predicted to be in a range which the SWCNT-FET device could measure. The SWCNT-FET device had an approximate bandwidth of 10^1 - 10^5 s^{-1}, corresponding to $k_{off} \sim 10^1 - 10^5$ s^{-1}, which matched the kinetics of the 3C6-

paclitaxel system (k_{on} = 10^{12} M^{-1} s^{-1}, k_{off} = 10^{4} s^{-1}). By contrast, most antibodies exhibiting K_d =10 nM that were measured by typical ligand binding assays demonstrated k_{on} = 10^{4} M^{-1} s^{-1} and k_{off} = 10^{-4} s^{-1} (31), kinetics slow enough for the limited speed of SPR or fluorescence but outside the range of SWCNT-FET devices. Thus, ligand binding assays are complementary methods to the SWCNT-FET method used here, since each method measures different timescales.

The effective K_d obtained in this experiment was 30 nM, slightly different from the ensemble-measured K_d=10 nM. This result was unsurprising given that previous studies showed some variation in equilibrium and kinetic binding characteristics between different molecules of the same protein (32).

The value of 1.8 obtained for the Hill coefficient, close to the theoretical limit of 2 corresponding to the number of binding sites, indicated a strong interaction between the two paclitaxel-binding sites on the 3C6 molecule. The strong cooperativity enhanced paclitaxel binding to the second site even at low concentrations by making the second binding more favorable, a conclusion supported by recent studies (33). This result corroborated the earlier suggestion that the bi-exponential distribution of unbound times resulted from binding to the second arm of the antibody. As mentioned above, the SWCNT biosensor is only sensitive to conformational changes within ~1nm of the CNT sidewall, limiting the sensitivity of the device to one binding site. Thus, the SWCNT biosensor could be indirectly sensitive to intra-antibody cooperativity.

Summary

The results presented here demonstrate the ability of SWCNT-FET biosensors to probe microsecond-scale details in binding kinetics, distinguish between mechanisms in receptor-ligand binding, and to measure ligand concentration in solution. Using this CNT biosensor, we determined that the 3C6-paclitaxel system exhibited binding kinetics approximating typical receptor-ligand binding, but with enough deviation to suggest a multi-step, rather than a single-step, binding interaction. Further analysis of 3C6-paclitaxel binding dynamics strongly suggested that the two arms of the 3C6 antibody molecule exhibited cooperative binding behavior. The proposed model for describing the overall binding rate also showed that this CNT biosensing method was bandwidth-limited, suggesting that greater accuracy could be obtained in experiments performed at higher bandwidth. This study describing the non-linear relationship between binding kinetics and ligand concentration provides a new way to investigate rapid receptor-ligand interactions and may lead to a deeper understanding of the mechanics behind receptor-ligand specificity.

REFERENCES

1. Holford TR, Davis F, Higson SP. Recent trends in antibody based sensors. Biosensors and Bioelectronics. 2012;34(1):12-24.

2. Yang XD, Corvalan JR, Wang P, Roy CMN, Davis CG. Fully human anti-interleukin-8 monoclonal antibodies: potential therapeutics for the treatment of inflammatory disease states. Journal of Leukocyte Biology. 1999;66(3):401-10.

3. Engvall E. [28] Enzyme immunoassay ELISA and EMIT. Methods in enzymology. 70: Elsevier; 1980. p. 419-39.

4. Conroy PJ, Hearty S, Leonard P, O'Kennedy RJ, editors. Antibody production, design and use for biosensor-based applications. Seminars in cell & developmental biology; 2009: Elsevier.

5. Organization WH. WHO Model List of Essential Medicines, 20th list, March 2017. World Health Organization; 2017.

6. Gelderblom H, Mross K, ten Tije AJ, Behringer D, Mielke S, van Zomeren DM, et al. Comparative pharmacokinetics of unbound paclitaxel during 1-and 3-hour infusions. Journal of Clinical Oncology. 2002;20(2):574-81.

7. Bignami GS, Mooberry SL. Monoclonal antibodies to taxanes that neutralize the biological activity of paclitaxel. Cancer Letters. 1998;126(2):127-33.

8. Yueh Jung Lee CP, inventor; Autotelic LLC, assignee. Methods, devices, and reagents for monitoring paclitaxel concentration in plasma for pharmacokinetic-guided dosing of paclitaxel2015.

9. Voskuil JLA. The challenges with the validation of research antibodies. F1000Res. 2017;6:161-.

10. Patel R, Andrien BA. Kinetic analysis of a monoclonal therapeutic antibody and its single-chain homolog by surface plasmon resonance. Analytical Biochemistry. 2010;396(1):59-68.

11. Bantz KC, Meyer AF, Wittenberg NJ, Im H, Kurtulus O, Lee SH, et al. Recent progress in SERS biosensing. Physical Chemistry Chemical Physics. 2011;13(24):11551-67.

12. Sasakawa H, Sakata E, Yamaguchi Y, Masuda M, Mori T, Kurimoto E, et al. Ultra-high field NMR studies of antibody binding and site-specific phosphorylation of alpha-synuclein. Biochemical and Biophysical Research Communications. 2007;363(3):795-9.

13. Coppari E, Santini S, Bizzarri AR, Cannistraro S. Kinetics and binding geometries of the complex between beta(2)-microglobulin and its antibody: An AFM and SPR study. Biophysical Chemistry. 2016;211:19-27.

14. Kelliher MT, Jacks RD, Piraino MS, Southern CA. The effect of sugar removal on the structure of the Fc region of an IgG antibody as observed with single molecule Forster Resonance Energy Transfer. Molecular Immunology. 2014;60(2):103-8.

15. Choi YK, Moody IS, Sims PC, Hunt SR, Corso BL, Perez I, et al. Single-Molecule Lysozyme Dynamics Monitored by an Electronic Circuit. Science. 2012;335(6066):319-24.

16. Olsen TJ, Choi Y, Sims PC, Gu OT, Corso BL, Dong CJ, et al. Electronic Measurements of Single-Molecule Processing by DNA Polymerase I (Klenow Fragment). Journal of the American Chemical Society. 2013;135(21):7855-60.

17. Choi Y, Olsen TJ, Sims PC, Moody IS, Corso BL, Dang MN, et al. Dissecting Single-Molecule Signal Transduction in Carbon Nanotube Circuits with Protein Engineering. Nano Letters. 2013;13(2):625-31.

18. Kim YG, Ho SO, Gassman NR, Korlann Y, Landorf EV, Collart FR, et al. Efficient site-specific Labeling of proteins via cysteines. Bioconjugate Chemistry. 2008;19(3):786-91.

19. Collins PG, Fuhrer MS, Zettl A. 1/f noise in carbon nanotubes. Applied Physics Letters. 2000;76(7):894-6.

20. Liu F, Bao MQ, Kim HJ, Wang KL, Li C, Liu XL, et al. Giant random telegraph signals in the carbon nanotubes as a single defect probe. Applied Physics Letters. 2005;86(16).

21. Liu F, Wang KL, Zhang DH, Zhou CW. Random telegraph signals and noise behaviors in carbon nanotube transistors. Applied Physics Letters. 2006;89(24).

22. Tian J, Stella VJ. Degradation of paclitaxel and related compounds in aqueous solutions II: Nonepimerization degradation under neutral to basic pH conditions. Journal of Pharmaceutical Sciences. 2008;97(8):3100-8.

23. Lerner MB, D'Souza J, Pazina T, Dailey J, Goldsmith BR, Robinson MK, et al. Hybrids of a Genetically Engineered Antibody and a Carbon Nanotube Transistor for Detection of Prostate Cancer Biomarkers. Acs Nano. 2012;6(6):5143-9.

24. Topinka MA, Rowell MW, Goldhaber-Gordon D, McGehee MD, Hecht DS, Gruner G. Charge Transport in Interpenetrating Networks of Semiconducting and Metallic Carbon Nanotubes. Nano Letters. 2009;9(5):1866-71.

25. Reuel NF, Bojo P, Zhang JQ, Boghossian AA, Ahn JH, Kim JH, et al. NoRSE: noise reduction and state evaluator for high-frequency single event traces. Bioinformatics. 2012;28(2):296-7.

26. Gevondyan NM, Volynskaia AM, Gevondyan VS. Four free cysteine residues found in human IgG1 of healthy donors. Biochemistry-Moscow. 2006;71(3):279-84.

27. Liu H, May K, editors. Disulfide bond structures of IgG molecules: structural variations, chemical modifications and possible impacts to stability and biological function. MAbs; 2012: Taylor & Francis.

28. Harris LJ, Skaletsky E, McPherson A. Crystallographic structure of an intact IgG1 monoclonal antibody11Edited by I. A. Wilson. Journal of Molecular Biology. 1998;275(5):861-72.

29. Wenk MR, Fahr A, Reszka R, Seelig J. Paclitaxel partitioning into lipid bilayers. Journal of pharmaceutical sciences. 1996;85(2):228-31.

30. Sims PC, Moody IS, Choi Y, Dong CJ, Iftikhar M, Corso BL, et al. Electronic Measurements of Single-Molecule Catalysis by cAMP-Dependent Protein Kinase A. Journal of the American Chemical Society. 2013;135(21):7861-8.

31. Schwesinger F, Ros R, Strunz T, Anselmetti D, Guntherodt HJ, Honegger A, et al. Unbinding forces of single antibody-antigen complexes correlate with their thermal dissociation rates. Proceedings of the National Academy of Sciences of the United States of America. 2000;97(18):9972-7.

32. Marx V. Finding the right antibody for the job. Nature Methods. 2013;10(8):703-7.

33. Hattori T, Lai D, Dementieva IS, Montano SP, Kurosawa K, Zheng YP, et al. Antigen clasping by two antigen-binding sites of an exceptionally specific antibody for histone methylation. Proceedings of the National Academy of Sciences of the United States of America. 2016;113(8):2092-7.